Graphene on Rh(111): Scanning tunneling and atomic force microscopies studies

E. N. Voloshina, Yu. S. Dedkov, S. Torbrügge, A. Thissen, and M. Fonin

Articles you may be interested in

Copper intercalation at the interface of graphene and Ir(111) studied by scanning tunneling microscopy
Appl. Phys. Lett. **105**, 191603 (2014); 10.1063/1.4901165

First-principles study for stability and binding mechanism of graphene/Ni(111) interface: Role of vdW interaction
J. Chem. Phys. **141**, 044708 (2014); 10.1063/1.4890728

Atomic and electronic structure of graphene/Sn-Ni(111) and graphene/Sn-Cu(111) surface alloy interfaces
Appl. Phys. Lett. **101**, 051602 (2012); 10.1063/1.4739475

Nucleation and growth of nickel nanoclusters on graphene Moiré on Rh(111)
Appl. Phys. Lett. **96**, 093115 (2010); 10.1063/1.3341176

Scanning tunneling microscopy on epitaxial bilayer graphene on ruthenium (0001)
Appl. Phys. Lett. **94**, 133101 (2009); 10.1063/1.3106057

Graphene on Rh(111): Scanning tunneling and atomic force microscopies studies

E. N. Voloshina,[1] Yu. S. Dedkov,[2,a)] S. Torbrügge,[2] A. Thissen,[2] and M. Fonin[3]

[1]*Physikalische und Theoretische Chemie, Freie Universität Berlin, 14195 Berlin, Germany*
[2]*SPECS Surface Nano Analysis GmbH, Voltastraße 5, 13355 Berlin, Germany*
[3]*Fachbereich Physik, Universität Konstanz, 78457 Konstanz, Germany*

The electronic and crystallographic structure of the graphene/Rh(111) moiré lattice is studied via combination of density-functional theory calculations and scanning tunneling and atomic force microscopy (STM and AFM). Whereas the principal contrast between *hills* and *valleys* observed in STM does not depend on the sign of applied bias voltage, the contrast in atomically resolved AFM images strongly depends on the frequency shift of the oscillating AFM tip. The obtained results demonstrate the perspectives of application atomic force microscopy/spectroscopy for the probing of the chemical contrast at the surface. © *2012 American Institute of Physics*. [http://dx.doi.org/10.1063/1.4729549]

Graphene, a single layer of carbon atoms ordered in a "chicken-wire" lattice,[1–3] is proposed to be used in many technological applications. Among them are gas sensors,[4] THz-transistors,[5] integrated circuits,[6] touch screens,[7] and many others.[1,3] One of the promising systems on the basis of graphene is its interface with metallic substrates.[8–10] Here, graphene can be used as a protection layer for the underlying substrate,[11–14] as a spin-filtering material separating two layers of a ferromagnetic material,[15–17] or, in case of its growth on a lattice mismatched surfaces [for example, Ir(111), Rh(111), or Ru(0001)], as a template for the preparation of ordered arrays of clusters.[18,19]

In the row of the graphene/metal lattice mismatched systems, the graphene/Rh(111) interface can be considered as an intermediate case between two systematically studied graphene-metal systems: graphene/Ir(111) and graphene/Ru(0001). These three interfaces represent the situation of a relatively large lattice mismatch between graphene and a metallic substrate. As was demonstrated, the moiré structure of graphene on Ir and Ru can be considered as two extreme cases of weakly and strongly interacting interfaces, respectively.[20–23] For graphene on Rh(111) [see Fig. 1(a)], several regions of different arrangements of carbon atoms above a Rh(111) substrate can be found. In this system, these regions are well pronounced and can be clearly separated. When using the common notations, the following high-symmetry places can be identified: *ATOP* [A; carbon atoms are placed above Rh(S-1) and Rh(S-2) atoms], *HCP* [H; carbon atoms are placed above Rh(S) and Rh(S-2) atoms], *FCC* [F; carbon atoms are placed above Rh(S) and Rh(S-1) atoms], and *BRIDGE* [B; Rh(S) atoms bridge the carbon atoms]. These places are marked in Fig. 1(a) by circle, down-triangle, square, and stars, respectively. Among them, the *BRIDGE* positions are expected to be the most energetically favorable for the nucleation of deposited atoms on top of a graphene layer. The nowadays available force spectroscopy and microscopy can shed light on this problem and can

be used as a tool, which helps to optimize the preparation of ordered arrays of clusters on a graphene template.[24]

In this manuscript, we present the combined study of the graphene/Rh(111) system via application of the state-of-the-art density-functional theory (DFT) calculations and scanning tunneling and atomic force microscopy (STM and AFM). The calculated imaging contrast for STM between all high-symmetry positions for graphene/Rh(111) is in very good agreement with experimental results, and this contrast does not depend on the sign of the bias voltage applied between a tip and the sample. As opposed to the latter observation, the imaging contrast in atomically resolved AFM measurements depends on the frequency shift of the oscillating tip, which can be understood on the basis of measured force-spectroscopy curves. The presented results are compared with the available theoretical data.

The presented in Fig. 1(a) crystallographic model of graphene/Rh(111) was used in DFT calculations, which were carried out using the projector augmented wave method,[25] a plane wave basis set with a maximum kinetic energy of 400 eV and the PBE-GGA exchange-correlation potential,[26] as implemented in the VASP program.[27] The long-range van der Waals interactions were accounted for by means of a semiempirical DFT-D2 approach proposed by Grimme.[28] The studied system is modeled using supercell, which has an (11×11) lateral periodicity and contains one layer of (12×12) graphene on four-layer slab of metal atoms (in total 772 atoms). Metallic slab replicas are separated by ca. 18 Å in the surface normal direction. To avoid interactions between periodic images of the slab, a dipole correction is applied.[29] The surface Brillouin zone is sampled with a single k-point at the Γ point for structure optimization and set to 3×3 in the total energy calculations. The STM images are calculated using the Tersoff-Hamann formalism,[30] in its most basic formulation, approximating the STM tip by an infinitely small point source.[31,32]

The graphene/Rh(111) system was prepared in ultra-high vacuum station for STM/AFM studies according to the recipe described in details in Refs. 19 and 33. The quality and homogeneity were verified by means of low-energy

a)Author to whom correspondence should be addressed. E-mail: Yuriy.Dedkov@specs.com.
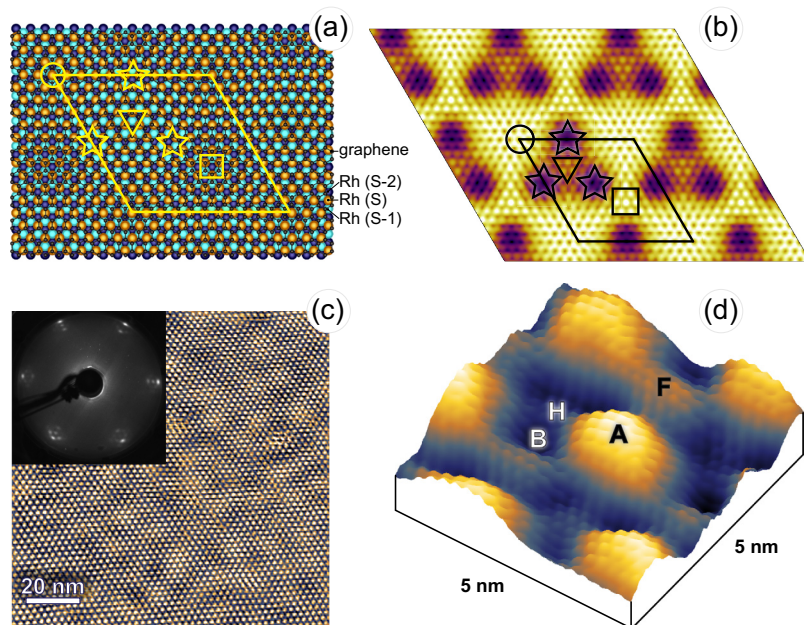
FIG. 1. (a) Crystallographic structure and (b) the corresponding calculated STM image of graphene/Rh(111). (c) Large scale STM image of the graphene layer on Rh(111). Tunneling conditions: $U_T = +1$ V, $I_T = 1$ nA. (d) 3D view of the 5×5 nm^2 region from (c) showing the structure of the graphene layer on Rh(111). Tunneling conditions: $U_T = -0.55$ V, $I_T = 10$ nA. The capital letters denote the corresponding high-symmetry adsorption sites of carbon atoms on Rh(111).

electron diffraction (LEED) and STM. The STM/AFM images were collected with Aarhus SPM 150 equipped with KolibriSensor^{TM} from SPECS (Ref. 34) with Nanonis Control system. In all measurements, the sharp W-tip was used which was cleaned *in situ* via Ar$^+$-sputtering. In presented STM images, the tunneling bias voltage, U_T, is referenced to the sample and the tunneling current, I_T, is collected by the tip, which is virtually grounded. During the AFM measurements the sensor was oscillating with the resonance frequency of $f_0 = 1\,001\,541$ Hz and the quality factor of $Q = 32\,323$, and the frequency shift was used as an input signal in a feedback loop for the topography measurements. The oscillation amplitude was set to $A = 300$ pm. The base vacuum was better than 8×10^{-11} mbar during all experiments. All measurements were performed at room temperature.

The DFT-D2 optimized structure is presented in Fig. 1(a) and the variation of the height of the carbon atoms is shown in Fig. S1 of the supplementary material.[35] Carbon atoms in the *ATOP* configuration define a high-lying region sitting at $d_0 = 3.15$ Å above Rh(111), and those in other configurations form a lower region. The buckling in the graphene overlayer is 1.07 Å. Carbon atoms in the *BRIDGE* configuration form the lowest topographic area ($d_0 = 2.08$ Å). The *HCP* and *FCC* regions are approximately 0.4 Å and 0.8 Å higher than the minima.

We have estimated the influence of dispersion forces on the obtained results: while qualitatively the observed picture remains the same, non inclusion of the van der Waals interactions (i.e., standard DFT-PBE treatment) yields larger corrugation (≈ 1.8 Å) with a very similar low region ($d_0 = 2.10$ Å), but a high region at $d_0 = 3.90$ Å. This is due to the alternating "weak" and "strong" interactions of graphene with the Rh(111) surface. In the case of the "strong" interaction between graphene and metal, standard GGA-treatment gives reasonable result, whereas for the areas of the "weakly" bonded graphene dispersion forces, neglected by the standard procedure, are important.

Fig. 1(b) shows the DFT-D2-calculated STM image (distance between graphene and the tunneling tip is $z = 2$ Å) of

the graphene layer on Rh(111). All structural replicas are clearly visible in calculated STM image, and they are marked by the corresponding symbols in Fig. 1(b). The brightest region in this image is the one surrounding the *ATOP* (A; circle) high symmetry arrangement for graphene on Rh(111). Here the graphene layer is most weakly bounded to the Rh substrate. The next two places in the bonding row are *FCC* (F; rectangle) and *HCP* (H; triangle). The darkest place in the calculated STM image is the *BRIDGE* (B; star) position of the carbon atoms above Rh(111), where the strongest interaction of graphene and Rh(111) is expected and was calculated.

Figs. 1(c) and 1(d) show the experimental STM images of the graphene/Rh(111) system collected over large area and several unit cells of the graphene layer on Rh(111), respectively. The LEED picture of this system is shown as an inset of (c). The results, presented in (d), are the part of the results shown in Fig. S2 of the supplementary material.[35] The presented data demonstrate the high quality of the studied system over large regions as well as locally and they are in very good agreement with the previously published results.[19,33,36] The brightest areas are the *ATOP* (A) positions and the darkest are the *BRIDGE* (B) ones. The clear and unique assignment of all arrangements of carbon atoms in the graphene layer and the Rh substrate can be made via comparison of experimental and theoretical data due to the extremely good agreement between them (Figs. 1 and S2 of the Supplementary material[35]). The corrugation of the graphene layer on Rh(111) was measured between 0.5 Å and 1.5 Å depending on the imaging conditions. However, the principal contrast in STM images is not changed upon variation of the tunneling conditions (see Fig. S3 in the supplementary material for the corresponding images[35]).

The more intriguing results were obtained by AFM imaging of the graphene/Rh(111) system and they are compiled in Fig. 2 and demonstrate the clear atomic contrast in atomic force microscopy images of graphene on Rh(111). In the beginning, the force spectroscopy of the studied surface was performed via monitoring the frequency shift of the oscillating tip as a function of the distance between the tip
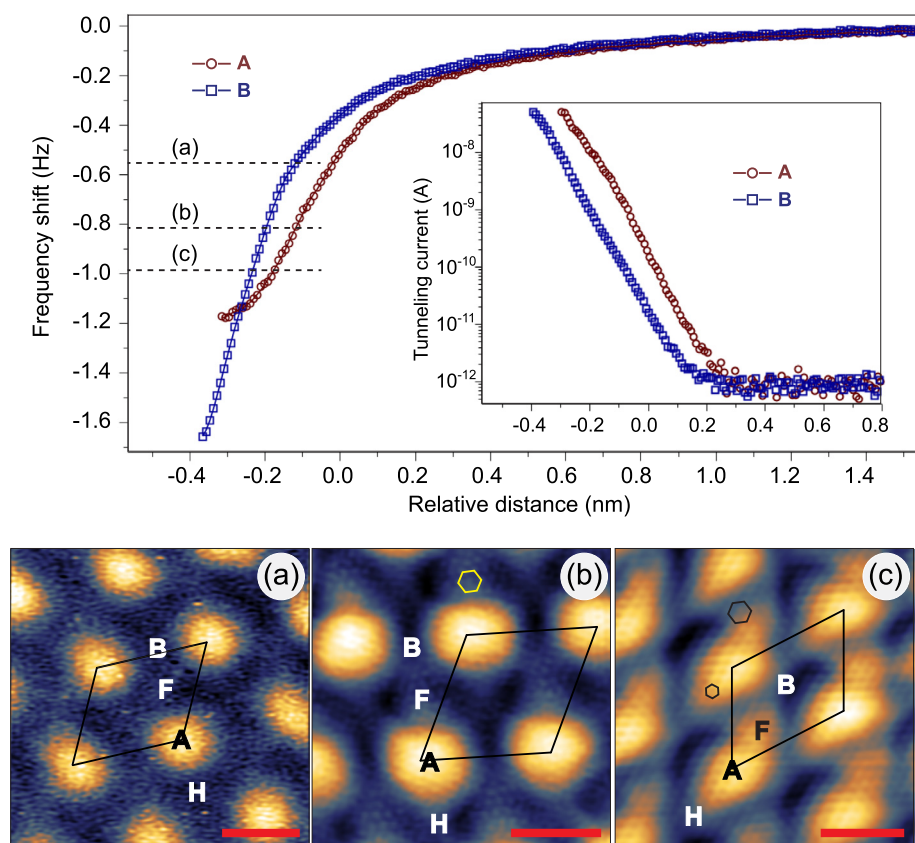
FIG. 2. (Upper panel) Frequency shift plots as functions of the relative distance with respect to the scanning position ($U_T = -840$ mV, $I_T = 0.48$ nA) for *hills* (A) and *valleys* (B). The inset shows the respective tunneling current, $I(z)$. (Lower panel) The AFM images measured at the frequency shifts of the sensor marked by the corresponding dashed lines in the upper panel. The large and small hexagons mark the graphene unit cell and the carbon ring, respectively. The distorted rhombuses mark the graphene moiré cell on Rh(111). The scale bar in the right lower conner of (a)–(c) is equal to 2 nm.

and the surface, $\Delta f(z)$. At the same time the tunneling current, $I(z)$, was collected. The representative curves for the two most contrast areas of the graphene/Rh(111) topography, namely *ATOP* and *BRIDGE*, are shown in the upper panel of Fig. 2 as open circles and squares, respectively. The corresponding force curves, $F(z)$, are shown in Fig. S4 of the supplementary material.[35] The tunneling current (shown as a semi-logarithmic plot in the inset of the upper panel of Fig. 2) demonstrates the exponential dependence on the distance between sample and the tip characteristic for two metallic electrodes separated by vacuum. The horizontal dashed lines indicate the frequency shifts for the KolibriSensor™ at which the AFM images were subsequently collected. These images with the pointing of the high symmetry stacking positions of graphene/Rh(111) are presented as a low row of Fig. 2 and marked by the corresponding letters.

The presented force curves can be clearly distinguished from each other that indicates the sensitivity of AFM to the different adsorption sites on the graphene layer on Rh(111). This difference in adsorption energies for different places in the graphene/Rh(111) lattice was pointed earlier in Ref. 37: it was found that the *ATOP* position is less energetically favorable for adsorption and there is a tendency for atoms to nucleate around the *BRIDGE* positions. These theoretical observations are supported by our experimental results: the expected equilibrium distance between tip and the sample for the *BRIDGE* position is smaller compared to the one for the *ATOP* position and the attractive part of the force [proportional to the frequency shift, $\Delta f(z)$] is large for the *BRIDGE* position. Thus, AFM imaging of the surface can be

used as a tool for precise detecting of the chemical and the electronic contrasts.

The interesting results are obtained when collecting AFM images at the frequency shifts marked in Fig. 2: increasing of the frequency shift during imaging leads to approaching the scanning tip closer to the studied surface that yields the increasing imaging contrast. This can be explained by the increasing of the contribution of chemical forces between tip and surface for shorter distances compared to mostly van der Waals forces for long distances between tip and surface. This effect is clearly visible in Figs. 2(a)–2(c). In (a), one can see the contrast only between "hills" and "valleys" of graphene/Rh(111), whereas in AFM images shown in (b) and (c) the evident difference between *ATOP*, *HCP*, *FCC*, *BRIDGE* positions (they are marked by the corresponding letters) as well as atomically resolved contrast in the graphene layer are visible. In all these AFM images [Figs. 2(a)–2(c)], the topography of the graphene/Rh(111) lattice as well as all height variations are well reproduced. For the discussion of the observed contrast between *HCP*, *FCC*, *BRIDGE* positions in the obtained AFM images [Fig. 2(d)] we can refer to Ref. 37 (see also Figs. S6 and S7 of the supplementary material[35] for the calculated site-projected density of states for carbon atoms and the difference of electron density at the graphene/Rh(111) interface, respectively), where the bonding of atoms of different nature on different adsorption sites of the graphene/Rh(111) is discussed. However, the more careful modeling and the further extended discussion is necessary here, which could be a topic of the future studies.

The closer look analysis of Figs. 2(b) and 2(c) and Fig. S5 of the supplementary material[35] shows that around "strongly" bonded regions of graphene on Rh(111) (*BRIDGE*, *HCP*, *FCC*) the full unit cell of graphene is imaged when only every second atom in the graphene unit cell is visible [larger hexagons in Figs. 2(b) and 2(c)]. This is a well known effect for the STM or AFM imaging of the graphite- or graphene-based systems. This effect is also clearly visible in our STM images (see discussion above and Fig. 1) analogous to the STM imaging of the graphene/Ni(111) system.[17,38] Increasing the frequency shift when one goes from image (b) to (c) leads to the increasing the imaging contrast and to the appearance of the atomically resolved contrast above *ATOP* positions, where now every carbon atom in the graphene unit cell can be resolved [smaller hexagon in Fig. 2(c)]. This is a demonstration of the fully resolved carbon ring of the strongly corrugated graphene layer on the metallic surface. The present effect can appear due to the local decoupling of graphene from the metallic substrate where the local hybridization between electron states of the graphene layer and the substrate is very small. A weak hybridization (if any) is also reflected in the carbon-atom-projected partial density of states (PDOS) and the difference of electron density at the graphene/Rh(111) interface (see also Figs. S6 and S7 of the supplementary material[35]). The corresponding PDOS for the carbon atoms around the *ATOP* position is very close to the one for the free-standing graphene for which the imaging of every single carbon atom in the unit cell was obtained.[39] (The positions of the peaks corresponding to σ- and π-states of graphene are shifted from approx. 3.5 eV and 6.5 eV of binding energy for the *ATOP* position to approx. 4.5 eV and 7.5 eV for the *BRIDGE* position, respectively, reflecting the different strength of hybridization between valence band states of graphene and Rh for two adsorption positions of carbon atoms.)

In conclusion, we present the studies of the graphene/Rh(111) system by means of DFT, STM, AFM, and force/tunneling current spectroscopy. The STM results show the perfect agreement with the theoretically calculated images and no principal difference in the contrast was found upon changing the sign of the bias voltage between the tip and the sample. On the contrary, the atomically resolved AFM results demonstrate the dependence on the imaging conditions, namely on the frequency shift of the sensor. The obtained AFM and STM results on graphene/Rh(111) are understood on the basis of the DFT-D2 calculations, and they demonstrate the high perspectives of AFM for the imaging of the chemical contrast in the graphene/metal systems.

[1] A. Geim, Science **324**, 1530 (2009).
[2] A. Geim, Rev. Mod. Phys. **83**, 851 (2011).
[3] K. Novoselov, Rev. Mod. Phys. **83**, 837 (2011).
[4] F. Schedin, A. K. Geim, S. V. Morozov, E. W. Hill, P. Blake, M. I. Katsnelson, and K. S. Novoselov, Nature Mater. **6**, 652 (2007).
[5] Y. M. Lin, C. Dimitrakopoulos, K. A. Jenkins, D. B. Farmer, H. Y. Chiu, A. Grill, and P. Avouris, Science **327**, 662 (2010).
[6] Y.-M. Lin, A. Valdes-Garcia, S.-J. Han, D. B. Farmer, I. Meric, Y. Sun, Y. Wu, C. Dimitrakopoulos, A. Grill, P. Avouris *et al.*, Science **332**, 1294 (2011).
[7] S. Bae, H. Kim, Y. Lee, X. Xu, J.-S. Park, Y. Zheng, J. Balakrishnan, T. Lei, H. R. Kim, Y. I. Song *et al.*, Nature Nanotech. **5**, 574 (2010).
[8] J. Wintterlin and M. L. Bocquet, Surf. Sci. **603**, 1841 (2009).
[9] M. Batzill, Surf. Sci. Rep. **67**, 83 (2012).
[10] Yu. S. Dedkov, K. Horn, A. Preobrajenskij, and M. Fonin, in *Graphene Nanoelectronics*, edited by H. Raza (Springer, Berlin, 2012), pp. 189–234.
[11] Yu. S. Dedkov, M. Fonin, and C. Laubschat, Appl. Phys. Lett. **92**, 052506 (2008).
[12] Yu. S. Dedkov, M. Fonin, U. Rüdiger, and C. Laubschat, Appl. Phys. Lett. **93**, 022509 (2008).
[13] E. Sutter, P. Albrecht, F. E. Camino, and P. Sutter, Carbon **48**, 4414 (2010).
[14] S. Chen, L. Brown, M. Levendorf, W. Cai, S.-Y. Ju, J. Edgeworth, X. Li, C. W. Magnuson, A. Velamakanni, R. D. Piner *et al.*, ACS Nano **5**, 1321 (2011).
[15] V. M. Karpan, G. Giovannetti, P. A. Khomyakov, M. Talanana, A. A. Starikov, M. Zwierzycki, J. van der Brink, G. Brocks, and P. J. Kelly, Phys. Rev. Lett. **99**, 176602 (2007).
[16] V. M. Karpan, P. A. Khomyakov, A. A. Starikov, G. Giovannetti, M. Zwierzycki, M. Talanana, G. Brocks, J. van der Brink, and P. J. Kelly, Phys. Rev. B **78**, 195419 (2008).
[17] Yu. S. Dedkov and M. Fonin, New J. Phys. **12**, 125004 (2010).
[18] A. T. N'Diaye, T. Gerber, C. Busse, J. Myslivecek, J. Coraux, and T. Michely, New J. Phys. **11**, 103045 (2009).
[19] M. Sicot, S. Bouvron, O. Zander, U. Rüdiger, Yu. S. Dedkov, and M. Fonin, Appl. Phys. Lett. **96**, 093115 (2010).
[20] A. T. N'Diaye, S. Bleikamp, P. J. Feibelman, and Th. Michely, Phys. Rev. Lett. **97**, 215501 (2006).
[21] E. Sutter, D. P. Acharya, J. T. Sadowski, and P. Sutter, Appl. Phys. Lett. **94**, 133101 (2009).
[22] C. Gong, G. Lee, B. Shan, E. M. Vogel, R. M. Wallace, and K. Cho, J. Appl. Phys. **108**, 123711 (2010).
[23] B. Wang, M.-L. Bocquet, S. Marchini, S. Günther, and J. Wintterlin, Phys. Chem. Chem. Phys. **10**, 3530 (2008).
[24] Y. Sugimoto, P. Pou, M. Abe, P. Jelinek, R. Pérez, S. Morita, and Ó. Custance, Nature **446**, 64 (2007).
[25] P. Blochl, Phys. Rev. B **50**, 17953 (1994).
[26] J. Perdew, K. Burke, and M. Ernzerhof, Phys. Rev. Lett. **77**, 3865 (1996).
[27] G. Kresse and J. Hafner, J. Phys.: Condens. Matter **6**, 8245 (1994).
[28] S. Grimme, J. Comput. Chem. **27**, 1787 (2006).
[29] J. Neugebauer and M. Scheffler, Phys. Rev. B **46**, 16067 (1992).
[30] J. Tersoff and D. Hamann, Phys. Rev. B **31**, 805 (1985).
[31] D. E. P. Vanpoucke and G. Brocks, Phys. Rev. B **77**, 241308 (2008).
[32] E. N. Voloshina, A. Generalov, M. Weser, S. Böttcher, K. Horn, and Yu. S. Dedkov, New J. Phys. **13**, 113028 (2011).
[33] M. Sicot, P. Leicht, A. Zusan, S. Bouvron, O. Zander, M. Weser, Yu. S. Dedkov, K. Horn, and M. Fonin, ACS Nano **6**, 151 (2012).
[34] S. Torbrügge, O. Schaff, and J. Rychen, J. Vac. Sci. Technol. B **28**, C4E12 (2010).
[35] See supplementary material at http://dx.doi.org/10.1063/1.4729549 for additional experimental and theoretical data as well as for details of analysis.
[36] B. Wang, M. Caffio, C. Bromley, H. Früchtl, and R. Schaub, ACS Nano **4**, 5773 (2010).
[37] B. Wang and M.-L. Bocquet, J. Phys. Chem. Lett. **2**, 2341 (2011).
[38] L. V. Dzemiantsova, M. Karolak, F. Lofink, A. Kubetzka, B. Sachs, K. von Bergmann, S. Hankemeier, T. O. Wehling, R. Frömter, H. P. Oepen, A. I. Lichtenstein, and R. Wiesendanger, Phys. Rev. B **84**, 205431 (2011).
[39] P. Lauffer, K. V. Emtsev, R. Graupner, Th. Seyller, L. Ley, S. A. Reshanov, and H. B. Weber, Phys. Rev. B **77**, 155426 (2008).